
RUDOLFV: A FOUNDATION MODEL BY PATHOLOGISTS FOR PATHOLOGISTS

PREPRINT

Jonas Dippel * † ^{1,2,3}, Barbara Feulner * ¹, Tobias Winterhoff * ¹, Simon Schallenberg⁸,
Gabriel Dernbach^{1,3,8}, Andreas Kuntz¹, Stephan Tietz¹, Timo Milbich¹, Simon Heinke¹,
Marie-Lisa Eich^{1,8}, Julika Ribbat-Idel¹, Rosemarie Krupar¹, Philipp Jurmeister^{6,7}, David Horst^{6,8},
Lukas Ruff¹, Klaus-Robert Müller † ^{2,3,4,5}, Frederick Klauschen † ^{3,6,7,8}, Maximilian Alber † ^{1,8}

¹ Aignostics, Germany

² Machine Learning Group, Technische Universität Berlin, Germany

³ BIFOLD – Berlin Institute for the Foundations of Learning and Data, Germany

⁴ Department of Artificial Intelligence, Korea University, Republic of Korea

⁵ Max-Planck Institute for Informatics, Germany

⁶ German Cancer Research Center (DKFZ) & German Cancer Consortium (DKTK), Berlin & Munich Partner Sites

⁷ Institute of Pathology, Ludwig-Maximilians-Universität München, Germany

⁸ Institute of Pathology, Charité – Universitätsmedizin Berlin, Germany

*† Equal Contribution, † Work done during internship at Aignostics

ABSTRACT

Histopathology plays a central role in clinical medicine and biomedical research. While artificial intelligence shows promising results on many pathological tasks, generalization and dealing with rare diseases, where training data is scarce, remains a challenge. Distilling knowledge from unlabelled data into a foundation model before learning from, potentially limited, labelled data provides a viable path to address these challenges. In this work, we extend the state of the art of foundation models for digital pathology whole slide images by semi-automated data curation and incorporating pathologist domain knowledge.

Specifically, we combine computational and pathologist domain knowledge (1) to curate a diverse dataset of 133k slides corresponding to 1.2 billion image patches covering data from different fixation, staining, and scanning protocols as well as data from different indications and labs across the EU and US, (2) for grouping semantically similar slides and tissue patches, and (3) to augment the input images during training. We evaluate the resulting model on a set of public and internal benchmarks and show that although our foundation model is trained with an order of magnitude less slides, it performs on par or better than competing models. We expect that scaling our approach to more data and larger models will further increase its performance and capacity to deal with increasingly complex real world tasks in diagnostics and biomedical research.

1 Introduction

Pathology plays a central role in clinical medicine for tissue-based diagnostics and in biomedical research as a basis for understanding cellular and molecular mechanisms of disease. While molecular and omics based data complement histological assessments, the microscopic evaluation of morphological changes has persisted as a key component of pathology. Consequently most digital pathology work focuses on whole slide image analysis.

Despite artificial intelligence (AI) having led to promising proof-of-concepts and applications (e.g., [1, 2, 3, 4, 5]), generalization and robustness are still a challenge when translating applications into clinical setups. Moreover, limited numbers of samples available for training pose a particular challenge in medicine, because the distribution of disease frequencies is highly skewed with only relatively few frequent and a large number of rare diseases. Therefore, generating

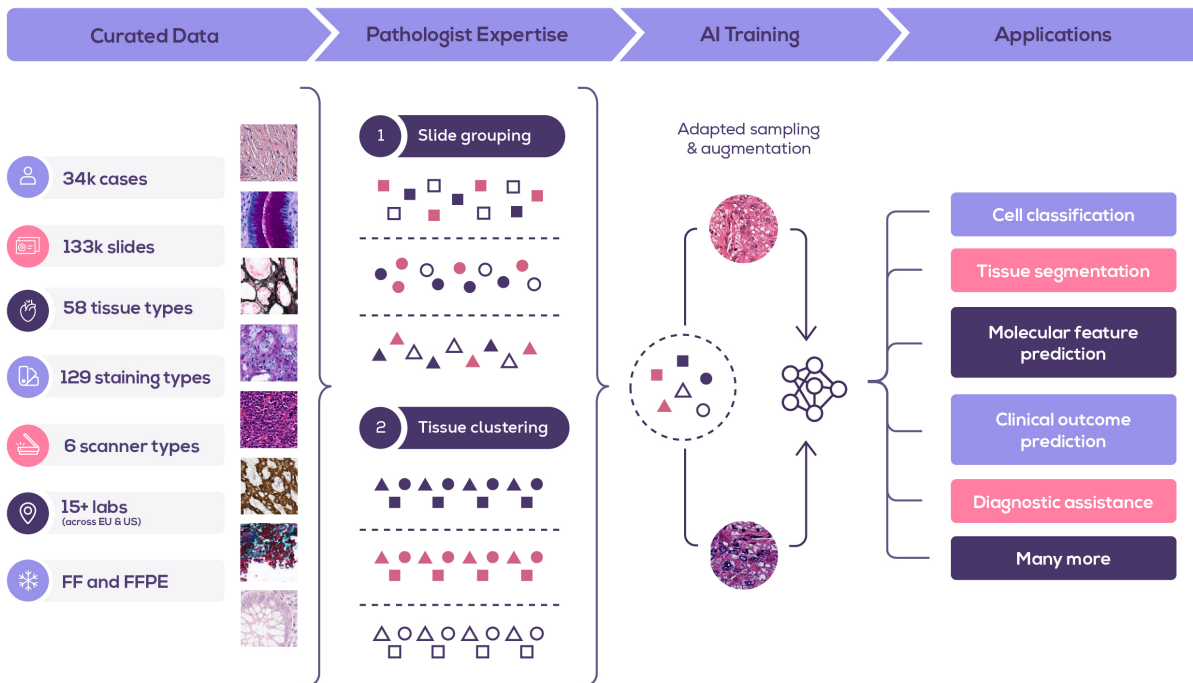


Figure 1: **(1) Curated data:** We curated a dataset of 133k slides with diverse properties. From these slides we extracted 1.2 billion image patches. **(2) Combining computational and pathologist expertise:** With Pathologist input, we grouped the slides into 31 groups, and - starting from a computer vision based clustering - the image patches into semantically meaningful tissue clusters. **(3) AI training:** We adapted DINOv2 training to sample a specific distribution of slide groups and tissue clusters and extend the augmentations with stain variations. **(4) Applications:** The resulting foundation model can be used for various applications in digital pathology.

enough labelled data to sufficiently cover observed variations regarding morphology, staining, scanner type, lab, and biology is (prohibitively) expensive.

Thus, while learning from labelled data will remain the standard for most AI use cases, strategies will be required to address the above outlined challenges. Here, foundation models [6] may contribute to a solution. This technique refers to pre-training a so-called foundation model on unlabelled data and to subsequently adapting it to learn from, potentially limited, labelled data. It typically uses the self-supervised learning (SSL, e.g., [7, 8, 9, 10]) paradigm and has shown breakthrough results in other domains when employed with an abundance of unlabelled data coupled with very large models (e.g., [11, 12, 13, 14, 8]).

Previous work successfully transferred foundation models to digital pathology images (e.g., [15, 16, 17, 18]), yet it falls short on incorporating crucial domain knowledge. In this work, we present an approach that integrates computational analysis and pathologist expertise into the data curation and training process. To the best of our knowledge, this is the first work to extensively incorporate pathology knowledge into foundation model development and to incorporate immunohistochemistry (IHC) and other non hematoxylin-and-eosin (H&E) stainings - which are important for many biomarker scoring use cases - into an SSL dataset. The presented approach reaches the best reported performance with an order of magnitude less slides and a smaller model than the current state of the art.

Our work is based on the assumption that optimally curated and more diverse data in connection with domain knowledge can improve SSL training. We therefore integrate pathologist knowledge in a number of key aspects. Specifically, we use pathologist input (1) to curate a dataset of 133k slides that covers diverse histological samples from different fixation, staining, and scanning protocols as well as data from different indications and labs from the EU and US, (2) for grouping semantically similar slides and tissue patches as well as (3) for augmenting the input images during training. Additional technical contributions are outlined in the methods section. We evaluate the resulting model on a set of public and internal benchmarks and compare it to latest related work.

Rudolf Virchow was not only the founder of modern pathology [19, 20, 21, 22], he was also the very founder of the institute our labs and most of the data for this work originate from. We therefore name our model "RudolfV" and join [18] in honoring his groundbreaking work and innovative spirit.

2 Related Work

In multiple works, self-supervised learning was adapted for training on histopathological images. Ciga et al. [23] trained on histopathological images with the SimCLR framework [7, 24]. The authors used multiple public data sources and showed that more diversity in pre-training data improves downstream task performance. Chen et al. trained a hierarchical model on 100 million image patches from TCGA slides (HIPT) [25] and showed that the DINO framework [26] and Vision Transformer (ViT) architecture [27] outperform other approaches [28]. The authors of CTransPath train a SwinTransformer [29] on 15 million images from TCGA and PAIP slides using a modified contrastive learning objective which mines additional semantically similar positive views (SRCL) [15]. Kang et al. [30] compare multiple self-supervised learning frameworks and find DINO to yield the best performance in a limited data setting. Remedis [31] first performs supervised training on natural images and then self-supervised pre-training on medical images. UNI [17] trains a ViT-L model on 100,000 slides with the DINOv2 framework [8] and provides extensive evaluations. Campanella et al. [32] train on 3 billion image patches from over 400,000 slides and compare masked autoencoder [9] and DINO self-supervised learning methods. Lastly, Virchow [18] is currently the best performing model, trained on over 1 million slides, also using the DINOv2 framework with a ViT-H/14 encoder.

So far none of the existing work, except Kang et al. [30], incorporates pathologist expertise in key aspects of the training process or uses non-HE stained data. Kang et al. [30] also use stain augmentation during training to diversify input images.

3 Data and Methods

Previous work (e.g., [33, 8, 23, 30, 34]) showed that data curation and domain knowledge are crucial for good model performance. For histopathological images, data curation can be done both on a whole slide level and on a tissue patch level. Considering that many slides contain potentially redundant properties such as regions with fatty or connective tissue or blood, we found it essential to also curate the tissue patch level data. Our approach performs filtering, grouping/clustering, and sampling for both levels with pathologists' expert input.

3.1 Data Curation

We curate a dataset focusing on data diversity both with respect to medical and technical aspects. The data across a broad range of disease entities was generated with different fixation, staining, scanning protocols, and in different labs across the EU and US. The dataset details are as follows:

- **Cases and slides:** The dataset consists of 133,998 slides comprising 34,103 cases. 108,433 (81%) slides have been chosen from our archive and 26,565 (19%) slides are from The Cancer Genome Atlas (TCGA).
- **Tissue location:** The tissue originates from 14 organ systems (Figure 2) comprising 58 different tissue types (examples for the granularity are lung, heart, adrenal gland, pancreas, oral cavity, bone marrow).
- **Labs:** The slides were created in over 15 different locations and labs in the EU and US.
- **Staining:** To the best of our knowledge, we are the first to combine H&E and non-H&E stainings. Our dataset contains 3 broad staining categories: H&E (68%), IHC (15%), and other (17%). Subdividing each staining category further results in 129 unique staining types. Examples are H&E, ER, PR, PD-L1, HER-2, Giemsa, PAS, Gomori, and others.
- **Scanning:** 6 different scanner types were used to scan the slides. This includes scanner types such as Roche Ventana DP600, Leica Aperio GT 450, and 3DHISTECH PANNORAMIC 1000. Scanning magnifications were typically 20x, 40x, and 80x.
- **Preparation:** The dataset contains both formalin-fixed-paraffin-embedded (FFPE) and fresh-frozen (FF) tissue samples.

From each slide we extract patches within given tissue boundaries derived from an in-house model. The patch size is 256×256 pixels at 0.5 mpp. This results in 1.25 billion image patches in total for further processing and training.

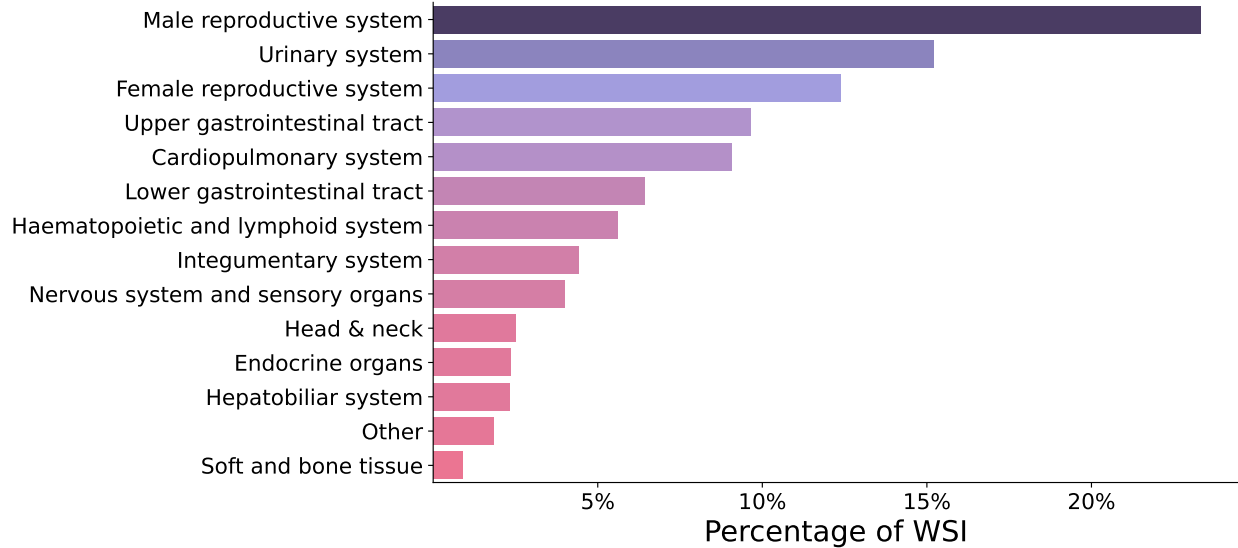


Figure 2: Distribution of tissue origin, where available, in terms of organ systems in our dataset of 133k whole slide images (WSI).

3.2 Slide Grouping and Tissue Clustering

Histological slides typically come with metadata available for data curation. Based on expert input as well as the sample’s lab of origin, tissue type, and staining, all slides were assigned to one of 31 groups. These groups are selected to maximize homogeneity within the groups and heterogeneity across the groups. During training we sample patches uniformly from these slide groups.

In contrast, individual tissue patches typically have no tissue specific metadata available. For optimizing patch sampling during training, we therefore create clusters based on computer vision image features and pathologist expertise. First, we extract 36 standard computer vision image features for all 1.25 billion image patches. These include image statistics such as mean and standard deviation for individual channels in common color modes such as RGB, LAB, HSV, and -tailored towards digital pathology - HED [35]. In contrast to [8], we do not use deep network features to reduce the computational burden. Next, we further reduce computational overhead by sub-sampling 500 patches for each slide and perform k-means clustering ($k = 100$) on the respective image features. We propagate the labels of the clustering via K-NN to assign a cluster label to each of the 1.25 billion patches. Finally, board-certified pathologists filter and aggregate the 100 image clusters assigning a description and a sampling probability (importance weight) to each cluster. This resulted in 9 distinct human-interpretable tissue clusters and 1.2 billion image patches after filtering irrelevant clusters. During training, we sample patches according to the sampling probability of the clusters. Within the clusters, we sample equally from the 31 slide groups.

3.3 Data Augmentation

In pathology, it is known that staining and scanning outputs vary between labs and even within the same lab over a given time period. Consequently in histopathology studies, staining and scanner information can produce spurious correlations and so-called “Clever Hans” effects [36] when it is correlated with label information [1]. To address this shortcoming, we transfer and augment stain and scanner color profiles in addition to the standard color augmentations in the view generation process of DINOv2. For each view, we pick a random other patch in the batch and normalize the image to the slide color statistics of the selected patch. This discourages the model from exploiting staining and scanner color features for learning representations.

We further add 90 degree rotations, horizontal, and vertical flipping to the augmentations in DINOv2 which adds the prior that objects on histopathological slides have no canonical orientation. Following [37, 30], we remove the solarization augmentation from the DINOv2 standard augmentations.

3.4 DINOv2

We build upon the official DINOv2 implementation [8] with registers [38]. DINOv2 learns representations via self-distillation and the final embedding representation is defined as in [18]. As [31] has shown that self-supervised histopathology models can benefit from pre-training on natural images, we initialize the student model with the distilled DINOv2 version pre-trained on LVD-142M [8]. This has shown to improve performance in smaller experimental setups. We train a ViT-L/14 with a batch size of 960 for 625k iterations.

4 Evaluation

We evaluate our model on a number of public and internal benchmarks.

4.1 Tasks

The benchmarks contain 9 different patch-based downstream tasks covering different tissue types, prediction tasks, and staining protocols.

PCAM, MHIST, CRC-100K benchmarks are an out-of-distribution validation for our model as the data was generated by separate labs. The internal HE and IHC tasks are an out-of-sample (or out-of-distribution, if indicated) validation for our model as we carefully separated cases from the pre-training and task datasets. For TIL Det., MSI CRC, MSI STAD there is a potential overlap between pre-training and task data, but we assume the impact to be negligible. Please note, similarly for CTransPath [15] and Phikon [16] it is unclear if pre-training and TIL Det., MSI CRC, MSI STAD task data overlap.

PCAM The PatchCamelyon dataset consists of 327,680 H&E images (96×96 pixels at 10x magnification) extracted from scans of lymph node sections of breast cancer. Each image is annotated with a binary label indicating presence of metastatic tissue. An image is labeled as metastatic tissue when one pixel was annotated as tumor [39, 40].

MHIST The MHIST dataset consists of 3,152 fixed-size H&E images (224×224 pixels at 8x magnification) of colorectal polyps. The task is to differentiate between hyperplastic polyp (HP) and sessile serrated adenoma (SSA). Each image is labeled according to the majority vote of seven pathologists. HPs are typically benign, while SSAs are precancerous lesions that can turn into cancer if left untreated and require sooner follow-up examinations [41].

CRC-100K The dataset contains 107,180 H&E images (224×224 pixels at 20x magnification) extracted from colorectal cancer scans. The task is to predict from each image the following 9 tissue classes: adipose, background, debris, lymphocytes, mucus, smooth muscle, normal colon mucosa, cancer-associated stroma, and colorectal adenocarcinoma epithelium. We use the unnormalized variant of the training dataset in our experiments (NCT-CRC-HE-100K-NONORM) [42, 43].

TIL Det. The pan-cancer tumor-infiltrating lymphocyte (TIL) detection dataset [44, 45] consists of 304,097 (209,221 training and 56,275 test) H&E images (100×100 pixels at 0.5mpp) extracted from scans of FFPE sections comprising 23 different cancer types from TCGA. The task is to predict TIL positive images. A TIL count higher than two indicates a positive image.

MSI CRC Microsatellite instability binary prediction on H&E colorectal cancer slides. The training split contains 74,726 image patches and the test split 98,904 image patches from TCGA slides. All image sizes are 224×224 pixels at 0.5 mpp [46, 47, 45].

MSI STAD Microsatellite instability binary prediction on H&E stomach adenocarcinoma slides. The training split contains 80,456 training and the test split 118,008 image patches from TCGA slides. All image sizes are 224×224 pixels at 0.5 mpp [46, 47, 45].

IHC cell classification (4 classes) The task is to predict the cell type at the center of an image patch (92×92 pixels at 0.5mpp). The four classes are carcinoma cell, lymphocyte, macrophage, and other. This internal benchmark dataset consists of 11,269, 3,218, and 1,609 board-certified pathologist annotated image patches taken from a larger corpora, split into train, validation, and test set respectively. The data is from 42 DAB-stained IHC slides of different cancer types, tissue locations and labs.

Pan-indication HE cell classification (5 indications, 8 classes) The task is to predict the cell type at the center of an image patch (128 × 128 pixels at 0.5mpp). The indications are urothelial cancer (UCa), breast cancer (BrCa), colorectal cancer (CRC), hepatocellular carcinoma (HCC) and non-small-cell lung cancer (NSCLC). The eight prediction classes are carcinoma cell, epithelial cell, plasma cell, fibroblast, lymphocyte, granulocyte, macrophage, and other. This internal benchmark dataset consists of 74,034, 24,692, and 70,198 board-certified pathologist annotated image patches taken from a larger corpora, split into train, validation, and test set respectively. The annotations are gathered from 347 slides of different tissue locations and labs. We created a hold out set for each indication consisting of cases not seen during training. For out-of-distribution evaluation we created a additional hold out dataset based on NSCLC cases from a different cohort and lab.

Pan-indication HE segmentation (3 indications, 5 classes) The task is semantic segmentation on an internal cohort, trained and evaluated on three indications: colorectal cancer (CRC), hepatocellular carcinoma (HCC) and non-small-cell lung cancer (NSCLC). From each slide we extract annotated patches at 0.5mpp. Depending on the model the patch input size was different: 224 pixels for the ImageNet based ViT and 336 pixels for the model from [16] and our model. For every pixel on the patch the model predicts one of the following classes: Carcinoma, Stroma, Ephemeral tissue, Necrosis or other. The training dataset originates from 456 slides of different tissue locations and labs, and is split into 30,553 train and 7,895 dev patches. We created a hold out set with a total of 11,800 patches, consisting of cases not seen during training. For out-of-distribution evaluation we created an additional hold out dataset based on NSCLC cases from a different cohort and lab.

4.2 Results

Public Classification Benchmarks: We evaluated all public benchmarks with linear probing. In line with related work [18], we do not use any augmentations on public benchmarks. During linear probing, we resize the images to 224 pixels and fit a linear classifier on the representations. We use the Adam optimizer with learning rate 5×10^{-5} , batch size 128 and cosine learning rate schedule.

Table 1: Linear probing benchmark results on public datasets. We report top-1 accuracy. * values are from [18, 30].

Model	PCAM	MHIST	CRC-100K	TIL Det.	MSI CRC	MSI STAD	Avg(1-3)	Avg(1-6)
ResNet50 ImageNet	0.833	0.806	0.849	0.915	0.653	0.664	0.829	0.786
ViT-L/16 ImageNet	0.852	0.796	0.847	0.924	0.669	0.671	0.832	0.793
Kang et al. [30]	0.918 *	0.771 *	0.949 *	0.943	0.745	0.756	0.879	0.847
CTransPath [15]	0.872 *	0.817 *	0.840 *	0.930	0.694	0.726	0.843	0.813
Phikon [16]	0.906 *	0.795 *	0.883 *	0.946	0.733	0.751	0.861	0.836
Virchow [18] ¹	0.933 *	0.834 *	0.968 *	-	-	-	0.912	-
Ours: RudolfV	0.944	0.821	0.973	0.943	0.755	0.788	0.913	0.871

The results of the public benchmarks in Table 1 show that our proposed approach yields better performance on all tasks except on the TIL detection and MHIST task, where Phikon [16] and Virchow [18] yield best performance respectively. Virchow [18] is not publicly available and could therefore not be included in all benchmarks.

We can observe a large performance gain compared to conventional ImageNet initialized models highlighting that in-domain pre-training can give a significant performance improvement. Staining and patch color are a confounding factor in task CRC-100K [1]. Our model outperforms all other models on this task, which can be an indication that stain augmentation helps to improve the stain invariance of foundation models.

Internal Classification Benchmarks: We evaluated all internal benchmarks with linear probing and finetuning. We extend the model embeddings with an additional linear layer and use mini-batch stochastic gradient descent with a logistic loss to train the models. For linear probing, the encoder weights are not updated and we use color augmentations during training for the HE task.

Table 2 and 3 show the evaluation results on internal HE classification benchmarks. Our proposed approach yields better results for all evaluation sets, both, for linear probing and for finetuning. For linear probing the model is on average 7 p.p. and for finetuning it is on average 5.6 p.p. better than the second best model Phikon[16]. On the out-of-distribution cohort the difference changes to 11.2 p.p and 4.8 p.p, respectively.

Table 2 and 3 also show the evaluation results on internal IHC classification benchmarks. Our proposed approach yields better results, both, for linear probing and for finetuning. For linear probing the model is 5.1 p.p. and for finetuning it is 3.4 p.p. better than the second best model Phikon[16].

¹We compare to the latest results of the Virchow preprint ([18], version 5).

Table 2: Model finetuning: Evaluation on internal cell classification benchmarks. All models are fully finetuned and we report macro-averaged balanced accuracy. OOD denotes an out-of-distribution evaluation.

Model	HE (5 indications, 8 classes)						Average	IHC (4 classes)
	UCa	BrCa	CRC	HCC	NSCLC	NSCLC OOD		
ResNet50 ImageNet	0.741	0.637	0.655	0.675	0.675	0.638	0.670	0.651
ViT-L/16 ImageNet	0.759	0.659	0.705	0.711	0.711	0.700	0.701	0.824
Phikon [16]	0.867	0.771	0.833	0.843	0.870	0.883	0.845	0.836
Ours: RudolfV	0.904	0.888	0.867	0.890	0.923	0.931	0.901	0.870

Table 3: Linear probing: Evaluation on internal cell classification benchmarks. For each model the encoder is frozen and only the linear classification head is trained. We report macro-averaged balanced accuracy. OOD denotes an out-of-distribution evaluation.

Model	HE (5 indications, 8 classes)						Average	IHC (4 classes)
	UCa	BrCa	CRC	HCC	NSCLC	NSCLC OOD		
ResNet50 ImageNet	0.282	0.239	0.217	0.222	0.232	0.225	0.236	0.291
ViT-L/16 ImageNet	0.470	0.402	0.382	0.371	0.423	0.316	0.394	0.423
Phikon [16]	0.776	0.648	0.679	0.582	0.744	0.682	0.685	0.637
Ours: RudolfV	0.848	0.689	0.754	0.644	0.800	0.794	0.755	0.688

Internal Segmentation Benchmarks: We evaluated all internal benchmarks in two modes, once with a frozen feature extractor and once with finetuning the entire model. We use a multi-layer segmentation head that operates exclusively on the patch embeddings of the encoder. We first bottleneck the embedding dimensionality, similar to [48], and then increase the spatial resolution by a factor of half the mini-patch size, using a bi-linear layer. Finally, we add a convolutional layer with the correct number of output channels, and upsample by a factor of two.

Table 4 and 5 show the evaluation results on internal segmentation benchmarks. Our proposed approach yields better results for all evaluation sets, both, for a frozen encoder and for finetuning. With a frozen encoder the model is on average 2.5 p.p. and when finetuning the whole model it is 2.6 p.p. better than the second best model Phikon[16]. On the out-of-distribution cohort the difference increases to 5.1 p.p and 6.5 p.p, respectively.

Table 4: Model finetuning: Evaluation on internal segmentation benchmarks. Every model is fully finetuned. We report macro-averaged balanced accuracy. OOD denotes an out-of-distribution evaluation.

Model	HE (3 indications, 5 classes)				
	NSCLC	NSCLC OOD	CRC	HCC	Average
ViT-L/16 ImageNet	0.786	0.669	0.888	0.812	0.789
Phikon [16]	0.905	0.778	0.945	0.897	0.881
Ours: RudolfV	0.912	0.843	0.962	0.910	0.907

Table 5: Frozen encoder: Evaluation on internal segmentation benchmarks. For each model the encoder is frozen and only the segmentation head is trained. We report macro-averaged balanced accuracy. OOD denotes an out-of-distribution evaluation.

Model	HE (3 indications, 5 classes)				
	NSCLC	NSCLC OOD	CRC	HCC	Average
ViT-L/16 ImageNet	0.703	0.577	0.806	0.723	0.702
Phikon [16]	0.891	0.782	0.931	0.891	0.874
Ours: RudolfV	0.910	0.833	0.946	0.908	0.899

5 Discussion and Future Work

This work shows that careful integration of pathological domain knowledge can lead to substantial performance gains with the - at the time of publication - best performing pathology foundation model, despite using an order of magnitude less slides and a model with less parameters than competing models. We assume that scaling the amount and diversity of data and the number of model parameters will further increase the performance of our approach. In follow-up work we will extend this manuscript with additional benchmarks, ablation studies, and increased data and model size.

We would like to note that while the present work is a machine learning focused study, we expect the results to be of great usefulness in future diagnostic real world settings and biomedical research. Future research will therefore explore exposing RudolfV to assisting clinical routine diagnostics in histopathology and more complex tasks including multimodal modeling.

Acknowledgement

We would like to thank the teams at Aignostics for supporting this work in many ways. Without their ground work this work would not have been possible.

The results shown here are in whole or part based upon data generated by the TCGA Research Network: <https://www.cancer.gov/tcga>.

References

- [1] Frederick Klauschen, Jonas Dippel, Philipp Keyl, Philipp Jurmeister, Michael Bockmayr, Andreas Mock, Oliver Buchstab, Maximilian Alber, Lukas Ruff, Grégoire Montavon, et al. Toward explainable artificial intelligence for precision pathology. *Annual Review of Pathology: Mechanisms of Disease*, 19:541–570, 2024.
- [2] James A Diao, Jason K Wang, Wan Fung Chui, Victoria Mountain, Sai Chowdary Gullapally, Ramprakash Srinivasan, Richard N Mitchell, Benjamin Glass, Sara Hoffman, Sudha K Rao, et al. Human-interpretable image features derived from densely mapped cancer pathology slides predict diverse molecular phenotypes. *Nature communications*, 12(1):1613, 2021.
- [3] Patricia Raciti, Jillian Sue, Juan A Retamero, Rodrigo Ceballos, Ran Godrich, Jeremy D Kunz, Adam Casson, Dilip Thiagarajan, Zahra Ebrahimzadeh, Julian Viret, et al. Clinical validation of artificial intelligence–augmented pathology diagnosis demonstrates significant gains in diagnostic accuracy in prostate cancer detection. *Archives of Pathology & Laboratory Medicine*, 147(10):1178–1185, 2023.
- [4] Alexander Binder, Michael Bockmayr, Miriam Hägele, Stephan Wienert, Daniel Heim, Katharina Hellweg, Masaru Ishii, Albrecht Stenzinger, Andreas Hocke, Carsten Denkert, et al. Morphological and molecular breast cancer profiling through explainable machine learning. *Nature Machine Intelligence*, 3(4):355–366, 2021.
- [5] Philipp Keyl, Michael Bockmayr, Daniel Heim, Gabriel Dernbach, Grégoire Montavon, Klaus-Robert Müller, and Frederick Klauschen. Patient-level proteomic network prediction by explainable artificial intelligence. *NPJ Precision Oncology*, 6(1):35, 2022.
- [6] Rishi Bommasani, Drew A Hudson, Ehsan Adeli, Russ Altman, Simran Arora, Sydney von Arx, Michael S Bernstein, Jeannette Bohg, Antoine Bosselut, Emma Brunskill, et al. On the opportunities and risks of foundation models. *arXiv preprint arXiv:2108.07258*, 2021.
- [7] Ting Chen, Simon Kornblith, Mohammad Norouzi, and Geoffrey Hinton. A simple framework for contrastive learning of visual representations. In *International conference on machine learning*, pages 1597–1607. PMLR, 2020.
- [8] Maxime Oquab, Timothée Darcet, Théo Moutakanni, Huy Vo, Marc Szafraniec, Vasil Khalidov, Pierre Fernandez, Daniel Haziza, Francisco Massa, Alaaeldin El-Nouby, et al. Dinov2: Learning robust visual features without supervision. *arXiv preprint arXiv:2304.07193*, 2023.
- [9] Kaiming He, Xinlei Chen, Saining Xie, Yanghao Li, Piotr Dollár, and Ross Girshick. Masked autoencoders are scalable vision learners. In *Proceedings of the IEEE/CVF conference on computer vision and pattern recognition*, pages 16000–16009, 2022.
- [10] Rayan Krishnan, Pranav Rajpurkar, and Eric J Topol. Self-supervised learning in medicine and healthcare. *Nature Biomedical Engineering*, 6(12):1346–1352, 2022.
- [11] Alec Radford, Jeffrey Wu, Rewon Child, David Luan, Dario Amodei, Ilya Sutskever, et al. Language models are unsupervised multitask learners. *OpenAI blog*, 1(8):9, 2019.
- [12] Tom Brown, Benjamin Mann, Nick Ryder, Melanie Subbiah, Jared D Kaplan, Prafulla Dhariwal, Arvind Neelakantan, Pranav Shyam, Girish Sastry, Amanda Askell, et al. Language models are few-shot learners. *Advances in neural information processing systems*, 33:1877–1901, 2020.
- [13] OpenAI. Gpt-4 technical report. *arXiv preprint arXiv:2303.08774*, 2023.

- [14] Tao Tu, Shekoofeh Azizi, Danny Driess, Mike Schaeckermann, Mohamed Amin, Pi-Chuan Chang, Andrew Carroll, Chuck Lau, Ryutaro Tanno, Ira Ktena, et al. Towards generalist biomedical ai. *arXiv preprint arXiv:2307.14334*, 2023.
- [15] Xiyue Wang, Sen Yang, Jun Zhang, Minghui Wang, Jing Zhang, Wei Yang, Junzhou Huang, and Xiao Han. Transformer-based unsupervised contrastive learning for histopathological image classification. *Medical image analysis*, 81:102559, 2022.
- [16] Alexandre Filiot, Ridouane Ghermi, Antoine Olivier, Paul Jacob, Lucas Fidon, Alice Mac Kain, Charlie Saillard, and Jean-Baptiste Schiratti. Scaling self-supervised learning for histopathology with masked image modeling. *medRxiv*, pages 2023–07, 2023.
- [17] Richard J Chen, Tong Ding, Ming Y Lu, Drew FK Williamson, Guillaume Jaume, Bowen Chen, Andrew Zhang, Daniel Shao, Andrew H Song, Muhammad Shaban, et al. A general-purpose self-supervised model for computational pathology. *arXiv preprint arXiv:2308.15474*, 2023.
- [18] Eugene Vorontsov, Alican Bozkurt, Adam Casson, George Shaikovski, Michal Zelechowski, Siqi Liu, Philippe Mathieu, Alexander van Eck, Donghun Lee, Julian Viret, et al. Virchow: A million-slide digital pathology foundation model. *arXiv preprint arXiv:2309.07778*, 2023.
- [19] Rudolf Virchow. Cellular pathology as based upon physiological and pathological histology... 1863.
- [20] David M Reese. Fundamentals–rudolf virchow and modern medicine. *Western journal of medicine*, 169(2):105, 1998.
- [21] Myron Schultz. Rudolf virchow. *Emerging infectious diseases*, 14(9):1480, 2008.
- [22] Constantin Goschler. *Rudolf Virchow: Mediziner-Anthropologe-Politiker*. Böhlau Köln, 2021.
- [23] Ozan Ciga, Tony Xu, and Anne Louise Martel. Self supervised contrastive learning for digital histopathology. *Machine Learning with Applications*, 7:100198, 2022.
- [24] Ting Chen, Simon Kornblith, Kevin Swersky, Mohammad Norouzi, and Geoffrey E Hinton. Big self-supervised models are strong semi-supervised learners. *Advances in neural information processing systems*, 33:22243–22255, 2020.
- [25] Richard J Chen, Chengkuan Chen, Yicong Li, Tiffany Y Chen, Andrew D Trister, Rahul G Krishnan, and Faisal Mahmood. Scaling vision transformers to gigapixel images via hierarchical self-supervised learning. In *Proceedings of the IEEE/CVF Conference on Computer Vision and Pattern Recognition*, pages 16144–16155, 2022.
- [26] Mathilde Caron, Hugo Touvron, Ishan Misra, Hervé Jégou, Julien Mairal, Piotr Bojanowski, and Armand Joulin. Emerging properties in self-supervised vision transformers. In *Proceedings of the IEEE/CVF international conference on computer vision*, pages 9650–9660, 2021.
- [27] Alexey Dosovitskiy, Lucas Beyer, Alexander Kolesnikov, Dirk Weissenborn, Xiaohua Zhai, Thomas Unterthiner, Mostafa Dehghani, Matthias Minderer, Georg Heigold, Sylvain Gelly, et al. An image is worth 16x16 words: Transformers for image recognition at scale. In *International Conference on Learning Representations*, 2020.
- [28] Richard J Chen and Rahul G Krishnan. Self-supervised vision transformers learn visual concepts in histopathology. *Learning Meaningful Representations of Life, NeurIPS 2021*, 2021.
- [29] Ze Liu, Yutong Lin, Yue Cao, Han Hu, Yixuan Wei, Zheng Zhang, Stephen Lin, and Baining Guo. Swin transformer: Hierarchical vision transformer using shifted windows. In *Proceedings of the IEEE/CVF international conference on computer vision*, pages 10012–10022, 2021.
- [30] Mingu Kang, Heon Song, Seonwook Park, Donggeun Yoo, and Sérgio Pereira. Benchmarking self-supervised learning on diverse pathology datasets. In *Proceedings of the IEEE/CVF Conference on Computer Vision and Pattern Recognition*, pages 3344–3354, 2023.
- [31] Shekoofeh Azizi, Laura Culp, Jan Freyberg, Basil Mustafa, Sebastien Baur, Simon Kornblith, Ting Chen, Nenad Tomasev, Jovana Mitrović, Patricia Strachan, et al. Robust and data-efficient generalization of self-supervised machine learning for diagnostic imaging. *Nature Biomedical Engineering*, pages 1–24, 2023.
- [32] Gabriele Campanella, Ricky Kwan, Eugene Fluder, Jennifer Zeng, Aryeh Stock, Brandon Veremis, Alexandros D Polydorides, Cyrus Hedvat, Adam Schoenfeld, Chad Vanderbilt, et al. Computational pathology at health system scale–self-supervised foundation models from three billion images. *arXiv preprint arXiv:2310.07033*, 2023.
- [33] Yonglong Tian, Olivier J Henaff, and Aäron van den Oord. Divide and contrast: Self-supervised learning from uncurated data. In *Proceedings of the IEEE/CVF International Conference on Computer Vision*, pages 10063–10074, 2021.

- [34] OpenAI: Josh Achiam et al. GPT-4 Technical Report, 2023.
- [35] Arnout C Ruifrok, Dennis A Johnston, et al. Quantification of histochemical staining by color deconvolution. *Analytical and quantitative cytology and histology*, 23(4):291–299, 2001.
- [36] Sebastian Lapuschkin, Stephan Wäldchen, Alexander Binder, Grégoire Montavon, Wojciech Samek, and Klaus-Robert Müller. Unmasking clever hans predictors and assessing what machines really learn. *Nature communications*, 10(1):1096, 2019.
- [37] Khrystyna Faryna, Jeroen Van der Laak, and Geert Litjens. Tailoring automated data augmentation to h&e-stained histopathology. In *Medical Imaging with Deep Learning*, 2021.
- [38] Timothée Darcet, Maxime Oquab, Julien Mairal, and Piotr Bojanowski. Vision transformers need registers. *arXiv preprint arXiv:2309.16588*, 2023.
- [39] Bastiaan S Veeling, Jasper Linmans, Jim Winkens, Taco Cohen, and Max Welling. Rotation equivariant CNNs for digital pathology. June 2018.
- [40] Babak Ehteshami Bejnordi, Mitko Veta, Paul Johannes Van Diest, Bram Van Ginneken, Nico Karssemeijer, Geert Litjens, Jeroen AWM Van Der Laak, Meyke Hermsen, Quirine F Manson, Maschenka Balkenhol, et al. Diagnostic assessment of deep learning algorithms for detection of lymph node metastases in women with breast cancer. *Jama*, 318(22):2199–2210, 2017.
- [41] Jerry Wei, Arief Suriawinata, Bing Ren, Xiaoying Liu, Mikhail Lisovsky, Louis Vaickus, Charles Brown, Michael Baker, Naofumi Tomita, Lorenzo Torresani, et al. A petri dish for histopathology image analysis. In *Artificial Intelligence in Medicine: 19th International Conference on Artificial Intelligence in Medicine, AIME 2021, Virtual Event, June 15–18, 2021, Proceedings*, pages 11–24. Springer, 2021.
- [42] Jakob Nikolas Kather, Johannes Krisam, Pornpimol Charoentong, Tom Luedde, Esther Herpel, Cleo-Aron Weis, Timo Gaiser, Alexander Marx, Nektarios A Valous, Dyke Ferber, et al. Predicting survival from colorectal cancer histology slides using deep learning: A retrospective multicenter study. *PLoS medicine*, 16(1):e1002730, 2019.
- [43] Jakob Nikolas Kather, Niels Halama, and Alexander Marx. 100,000 histological images of human colorectal cancer and healthy tissue, May 2018.
- [44] Jakub R Kaczmarzyk, Shahira Abousamra, Tahsin Kurc, Rajarsi Gupta, and Joel Saltz. Dataset for tumor infiltrating lymphocyte classification (304,097 image patches from TCGA), June 2022.
- [45] Jakub R Kaczmarzyk, Rajarsi Gupta, Tahsin M Kurc, Shahira Abousamra, Joel H Saltz, and Peter K Koo. Champkit: a framework for rapid evaluation of deep neural networks for patch-based histopathology classification. *Computer Methods and Programs in Biomedicine*, page 107631, 2023.
- [46] Jakob Nikolas Kather, Alexander T Pearson, Niels Halama, Dirk Jäger, Jeremias Krause, Sven H Loosen, Alexander Marx, Peter Boor, Frank Tacke, Ulf Peter Neumann, et al. Deep learning can predict microsatellite instability directly from histology in gastrointestinal cancer. *Nature medicine*, 25(7):1054–1056, 2019.
- [47] Jakob Nikolas Kather. Histological images for MSI vs. MSS classification in gastrointestinal cancer, FFPE samples, February 2019.
- [48] Alexander Kirillov, Eric Mintun, Nikhila Ravi, Hanzi Mao, Chloe Rolland, Laura Gustafson, Tete Xiao, Spencer Whitehead, Alexander C Berg, Wan-Yen Lo, et al. Segment anything. In *Proceedings of the IEEE/CVF International Conference on Computer Vision*, pages 4015–4026, 2023.